A&A 415, 705–715 (2004)
DOI: 10.1051/0004-6361:20034233
© ESO 2004

Astronomy & Astrophysics

The damping of slow MHD waves in solar coronal magnetic fields

II. The effect of gravitational stratification and field line divergence

I. De Moortel and A. W. Hood

School of Mathematics and Statistics, University of St Andrews, North Haugh, St Andrews, Fife KY16 9SS, Scotland, UK

Received 27 August 2003 / Accepted 12 November 2003

Abstract. This paper continues the study of De Moortel & Hood (2003) into the propagation of slow MHD waves in the solar corona. Firstly, the damping due to optically thin radiation is investigated and compared to the effect of thermal conduction. In a second stage, gravitational stratification is included in the model and it is found that this increases the damping length significantly. Finally, the effect of different magnetic field geometries on the damping of the slow waves is investigated. As a first approximation, a purely radial magnetic field is considered and although the amplitudes of the perturbations decrease due to the divergence of the field, the effect is small compared to the effect of thermal conduction. A more realistic local geometry, estimated from the observations, is investigated and it is demonstrated that a general area divergence can cause a significant, additional, decrease of the amplitudes of the perturbations. The results of numerical simulations, incorporating the effects of gravitational stratification, the magnetic field geometry and thermal conduction are compared with TRACE observations of propagating waves in coronal loops. It is found that a combination of thermal conduction and (general) area divergence yields detection lengths that are in good agreement with observed values.

Key words. Sun: oscillations – Sun: corona – Sun: activity

1. Introduction

Although the theoretical possibility of "coronal seismology" was suggested almost two decades ago (Roberts et al. 1984), it is only now that space based observations by satellites such as SOHO (*SOlar and Heliospheric Observatory*) and TRACE (*Transition Region And Coronal Explorer*) enable us to truly develop this idea. Indeed, slowly but surely, observational examples of all the different types of MHD waves are being discovered. In this paper, we will concentrate on periodic intensity disturbances that are observed to propagate along coronal loops. Similar density variations were first detected in coronal plumes by Ofman et al. (1997) using UVCS/SOHO and later by DeForest & Gurman (1998) using EIT/SOHO observations of polar plumes. These observations were interpreted as slow magneto-acoustic waves, propagating along coronal plumes, and Ofman et al. (1999, 2000a) showed that these waves could contribute significantly to the heating of the corona by viscous dissipation. A few years later, similar intensity disturbances were discovered in coronal loops in the EIT/SOHO 195 Å passband (Berghmans & Clette 1999) and in the TRACE 171 Å passband (De Moortel et al. 2000). A comparison of the properties of the density variations in the EIT/SOHO 195 Å and TRACE 171 Å passbands was presented by Robbrecht et al. (2001) and King et al. (2003). Based on these observations, Nakariakov et al. (2000) constructed a model, again in terms of slow magneto-acoustic waves and found that, for the observationally detected parameters, dissipation and gravitational stratification are the main factors influencing the wave evolution. The model was further developed by Tsiklauri & Nakariakov (2001), who incorporated the effect of a non-zero inclination angle and a semi-circular loop offset and showed that both the non-zero loop inclination and the offset decrease the growth of the wave amplitude due to stratification. These authors also show that wide-spectrum slow magneto-acoustic waves could provide a sufficient rate of heat deposition to heat the coronal loops in which the perturbations are observed. A similar study was carried out earlier by Erdélyi (1996). An extensive overview of the properties of longitudinal intensity oscillations observed in coronal loops, together with a discussion of the measured parameters was recently presented by De Moortel et al. (2002a,b). De Moortel et al. (2002c) demonstrated that the periodicity of the observed intensity variations can be divided into two distinct categories. Indeed, periods found in loops above sunspots are of the order of 3 min, whereas periods in non-sunspot loops are about 5 min.

Combining different instruments, several authors have now found observational evidence of slow magneto-acoustic waves propagating through the transition region and into the corona. Using mainly CDS/SOHO, MDI/SOHO and TRACE, O'Shea et al. (2002) found oscillations present in a sunspot umbra at all investigated temperatures, from the temperature

Send offprint requests to: I. De Moortel,
e-mail: ineke@mcs.st-and.ac.uk

Article published by EDP Sciences and available at http://www.aanda.org or http://dx.doi.org/10.1051/0004-6361:20034233

minimum (TRACE 1700 passband) to the coronal temperature of $\log T = 6.4$ K (CDS FE XVI 335 Å). The measured propagation speeds suggest that the observed oscillations are slow magneto-acoustic waves propagating up along the magnetic field lines. From a joint SOHO and TRACE observing campaign, Brynildsen et al. (2002) also found evidence for a 3 min period oscillation above a sunspot umbra. The oscillation amplitudes are found to increase with increasing temperature, reaching a maximum at about $1-2 \times 10^5$ K and then decreasing again in the higher temperature lines. These authors again suggest that wave propagation along the magnetic field above a sunspot region makes it possible for the 3 min oscillations to reach the corona. Recently, Marsh et al. (2003) found evidence for 5 min, propagating oscillations in CDS (He I, O V, Mg IX) observations of a non-sunspot region. This result again suggests propagating oscillations at chromospheric, transition region and coronal temperatures.

In this paper, we continue the investigation of the properties of uncoupled slow MHD waves, from the point of view of boundary driven oscillations. A theoretical study of the properties of MHD waves can be found in e.g. Porter et al. (1994a,b) and Roberts (2000, 2003). De Moortel & Hood (2003) (Paper I) compared the effect of thermal conduction and compressive viscosity and found that, for the observed coronal conditions, thermal conduction appears to be the dominant damping mechanism. However, there is a minimum damping length that can be obtained by thermal conduction alone, so if stronger damping is observed, an additional mechanism has to be found. Extending the model presented in Paper I, we now concentrate on the effect of gravitational stratification and the geometry of the magnetic field. In Sect. 2, we look at dissipation due to optically thin radiation, which was neglected in Paper I. Subsequently, the effect of density stratification along the loop (Sect. 3) and field line divergence (Sect. 4) are investigated. Following these general descriptions, specific observations are modelled (Sect. 5). Conclusions are presented in Sect. 6.

2. Optically thin radiation

In this paper we follow the analysis of De Moortel & Hood (2003). As we only consider the slow MHD oscillations, we restrict our attention to motions along the background, potential, magnetic field, which is directed along the z-axis. In this case, the MHD equations reduce to a 1D system of the form

$$\rho\frac{\partial v}{\partial t} + \rho v\frac{\partial v}{\partial z} = -\frac{\partial p}{\partial z}, \tag{1}$$

$$\frac{\partial \rho}{\partial t} = -\frac{\partial}{\partial z}(\rho v), \tag{2}$$

$$\frac{\partial p}{\partial t} + v\frac{\partial p}{\partial z} = -\gamma p\frac{\partial v}{\partial z} + (\gamma-1)\frac{\partial}{\partial z}\left(\kappa_\parallel\frac{\partial T}{\partial z}\right) - (\gamma-1)\left[\rho^2\chi T^\alpha - H_0\right], \tag{3}$$

$$p = \frac{1}{\tilde{\mu}}\rho R T, \tag{4}$$

where ρ is the mass density, p the gas pressure, T the temperature, v the velocity parallel to the magnetic field, $\kappa_\parallel = \kappa_0 T^{5/2}$ W m^{-1} deg^{-1} the thermal conductivity parallel to the magnetic field, R the gas constant and $\tilde{\mu}$ the mean molecular weight. The optically thin radiation is approximated by a piecewise continuous function, where χ and α are temperature dependent (Priest 1982, p. 88). The basic equilibrium is taken as a uniform plasma with pressure, p_0, density, ρ_0, and temperature, T_0. Finally, $H_0 = \rho_0^2\chi T_0^\alpha$ is the unknown coronal heating function. It is assumed fixed and maintains the equilibrium temperature, but does not contribute to the linearised, perturbation equations. In Paper I, we showed that compressive viscosity only has a minor effect on the propagation of slow MHD waves under the required coronal conditions (see Eq. (7)) and hence, we will neglect compressive viscosity in our present analysis. We remind the reader that, for a low-β plasma, the slow waves are essentially sound waves, guided by the magnetic field. The finite β correction can be obtained by exanding the linearised MHD equations in powers of β (Del Zanna et al. 1997). However, the order β correction is for the perpendicular components of the perturbations to the magnetic field and velocity. Hence, they are not important in the present study of longitudinal perturbations. Equations (1) to (4) are made dimensionless using the equilibrium values for pressure, density and temperature so that the velocity is given by $v = c_s\bar{v}$, where $c_s^2 = \frac{\gamma p_0}{\rho_0}$ is the adiabatic sound speed. Length and time are non-dimensionalised in terms of a distance L and time τ, where $L = c_s\tau$. The dimensionless equations contain the following dimensionless parameters, namely the thermal ratio, defined in Paper I as

$$d = \frac{(\gamma-1)\kappa_\parallel T_0\rho_0}{\gamma^2 p_0^2\tau} = \frac{1}{\gamma}\frac{\tau_s}{\tau_{\rm cond}}, \tag{5}$$

and the radiation ratio

$$r = \frac{(\gamma-1)\tau\rho_0^2\chi T_0^\alpha}{\gamma p_0} = \frac{\tau_s}{\tau_{\rm rad}}, \tag{6}$$

which is the ratio of the sound travel time ($\tau_s = L/c_s$) and the radiation timescale ($\tau_{\rm rad} = \gamma p_0/(\gamma-1)\rho_0^2\chi T_0^\alpha$). Notice that d and r are expressed in terms of the timescale τ. This is preferrable since most observed waves have a prescribed period, which we take as τ, rather than a prescribed coronal loop length. Using these expressions for d and r and assuming standard coronal values for all variables,

$$\begin{cases} T_0 = 10^6 \text{ K}, \\ \rho_0 = 1.67\times10^{-12} \text{ kg m}^{-3}, \\ \kappa_\parallel = 10^{-11}\, T_0^{5/2} \text{ W m}^{-1} \text{ deg}^{-1}, \\ \tilde{\mu} = 0.6, \\ \mathcal{R} = 8.3\times10^3 \text{ m}^2 \text{ s}^{-2} \text{ deg}^{-1}, \\ \gamma = 5/3, \\ \tau = 300 \text{ s}, \end{cases} \tag{7}$$

gives a value of $d = 0.025$ for the thermal ratio and $r = 0.06$ for the radiation ratio.

Dropping bars from dimensionless quantities, the linearised MHD equations are given by

$$\frac{\partial v_1}{\partial t} = -\frac{1}{\gamma}\frac{\partial p_1}{\partial z}, \tag{8}$$

$$\frac{\partial \rho_1}{\partial t} = -\frac{\partial v_1}{\partial z}, \tag{9}$$

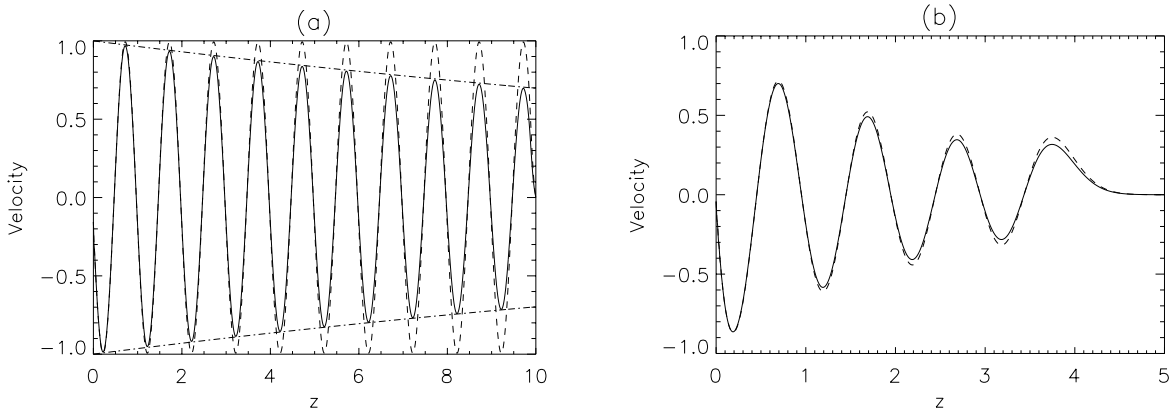

Fig. 1. a) A cross-section of the perturbed velocity as a function of z at $t = 10$, for which $z_{\max} = 15$, $d = 0$, $r = 0.06$ and for which the boundary was driven continuously. The dashed line shows the result for $r = 0$. The dot-dashed line shows the $\exp(-rz/\gamma)$ damping rate. **b)** Similar to **a)** but at $t = 4$ and with $z_{\max} = 5$ and $d = 0.025$.

$$\frac{\partial T_1}{\partial t} = -(\gamma - 1)\frac{\partial v_1}{\partial z} + \gamma d\frac{\partial^2 T_1}{\partial z^2} - r\,(2\rho_1 + \alpha T_1)\,, \tag{10}$$

$$p_1 = \rho_1 + T_1. \tag{11}$$

The effect of optically thin radiation depends on the value of α and the magnitude of ρ_1 to T_1. The T_1 term will destabilise if α is negative (Hood & Priest 1980; Field 1965).

The boundary conditions and initial conditions are chosen as in Paper I, namely,

$$v_1(z,0) = p_1(z,0) = \rho_1(z,0) = T_1(z,0) = 0, \tag{12}$$

and

$$v_1(0,t) = f(t), \qquad \frac{\partial p_1}{\partial z}(0,t) = -f'(t), \tag{13}$$

$$v_1(z_{\max},t) = 0, \qquad \frac{\partial p_1}{\partial z}(z_{\max},t) = 0, \tag{14}$$

$$T_1(0,t) = T_1(z_{\max},t) = 0, \tag{15}$$

where $f(t) = \sin(2\pi t)$. The partial differential equations will be solved using a simple, second-order, Lax-Wendroff scheme.

Consider the case when $\epsilon = 0$, i.e. no thermal conduction. Eqs. (8) to (11) can be combined to give

$$\frac{\partial^3 v}{\partial t^3} = \frac{\partial^3 v}{\partial t \partial z^2} - \frac{2r}{\gamma}\frac{\partial^2 v}{\partial z^2}. \tag{16}$$

Setting $v \sim \exp(\mathrm{i}(\omega t - kz))$ and substituting this expression into Eq. (16), we find

$$k = \left(\frac{\omega^3}{\omega + \mathrm{i}2r/\gamma}\right)^{1/2} \approx \omega\left(1 - \mathrm{i}\frac{r}{\gamma\omega}\right), \tag{17}$$

or, $v \sim \exp(\mathrm{i}\omega(t - z))\exp(-rz/\gamma)$. Hence, optically thin radiation will cause the amplitude of the velocity perturbations to decrease as $\exp(-rz/\gamma)$. Finally, we mention that a background instability is present when radiation is included in the model. However, the instability occurs on a time scale that is much longer than the time scales we are interested in. This is the usual, isobaric, thermal instability of Field (1965), in which the normal mode grows exponentially in time. The (isobaric) normal mode is only realised after the waves have reflected off the boundary at $z_{\max}$ and the pressure perturbations decreased. Here, the initial, transient disturbances are damped by radiation.

Figure 1a shows a cross-section of the perturbed velocity as a function of z at a constant time, driven with an infinite harmonic wavetrain. No thermal conduction was included, i.e. $d = 0$, and a value of $r = 0.06$ was used for the radiation ratio. The dashed line shows the result in an ideal plasma, i.e. for $d = r = 0$. It is clear that including optically thin radiation causes the amplitude of the velocity perturbations (solid line) to decrease, whereas the amplitude of the perturbations in the ideal plasma (dashed line) remain constant. The dot-dashed line confirms the $\exp(-rz/\gamma)$ damping rate obtained above. However, for this particular value of the radiation coefficient r, the damping due to optically thin radiation does not appear to be very effective. Indeed, for the values given in Eq. (7), the amplitude of the perturbations, at $z = 100$ Mm, has only dropped to about 92.5% of the initial value (see Table 1). In Fig. 1b we have included both thermal conduction and optically thin radiation, using the "standard" values of $d = 0.025$ and $r = 0.06$ for the thermal ratio and radiation ratio, respectively. The dashed line shows the result when optically thin radiation is neglected, and only thermal conduction is included. It is clear that including optically thin radiation causes some additional damping (an extra ~3.5% at 100 Mm, Table 1), but the effect is almost negligible under the chosen coronal conditions. However, due to the relatively low temperature, this is not surprising. At higher temperatures, of the order of 10 MK, the effect of optically thin radiation may become more important. Also, the footpoints of the observed loops are likely to be rooted in the chromosphere (which is not included in the present model), and hence, non-equilibrium ionisation might be important. Combined with the result of De Moortel & Hood (2003), this implies that thermal conduction appears to be the dominant dissipation mechanism for slow MHD waves, propagating in an non-stratified, non-diverging medium, at a temperature of 1 MK. Therefore, when investigating the effect of gravitational stratification and the magnetic field geometry, we will only consider thermal conduction, or, in other words, we set $r = 0$ from now on.

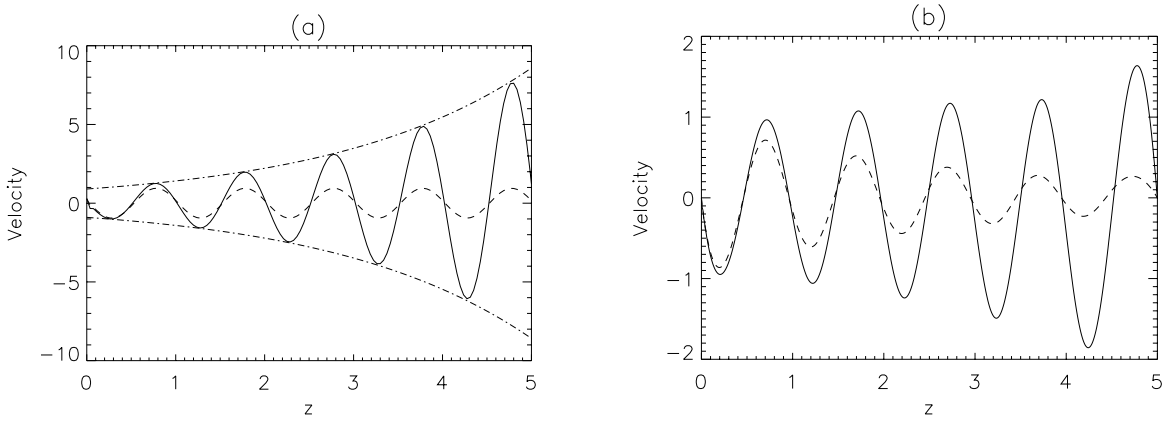

Fig. 2. a) A cross-section of the perturbed velocity as a function of z at $t = 10$, for which $z_{\max} = 15$, $d = 0$ and for which the boundary was driven continuously. The dashed line shows the result for an unstratified plasma. The dot-dashed line shows the $\exp(z/2H)$ growth rate. **b)** Similar to **a)** but at $t = 4$ and with $z_{\max} = 5$ and $d = 0.025$.

Table 1. The relative amplitude of the velocity perturbations, as a percentage of the amplitude of the basic model, at a distance of 100 Mm along the loop.

	Velocity perturbation at 100 Mm	
	Without thermal conduction	With thermal conduction
Basic model	100%	46.8%
Compressive viscosity	99.9%	44.7%
Optically thin radiation	92.5%	43.2%
Gravitational stratification	258.2%	130.5%
Radial area divergence	86.3%	40.6%
General area divergence	19.6%	9.7%
Strat. + Area div.	(55.6%)	26.1%

3. Gravitational stratification

Including gravity in our (isothermal), 1D model, will result in a background density and pressure of the form $\rho_0 = \rho_{00}\exp(-z/H)$ and $p_0 = p_{00}\exp(-z/H)$, respectively, where H is the gravitational scale height. Similar to Sect. 2, the dimensionless MHD equations are given by

$$\rho_0\frac{\partial v_1}{\partial t} = -\frac{1}{\gamma}\frac{\partial p_1}{\partial z} - \frac{\rho_1}{\gamma H}, \tag{18}$$

$$\frac{\partial \rho_1}{\partial t} + \frac{\partial}{\partial z}(\rho_0 v_1) = 0, \tag{19}$$

$$\frac{\partial T_1}{\partial t} = \frac{\partial}{\partial z}(\rho_0 v_1) - v_1\frac{\partial p_0}{\partial z} - \gamma p_0\frac{\partial v_1}{\partial z} + \gamma d\frac{\partial^2 T_1}{\partial z^2}, \tag{20}$$

$$p_1 = \rho_1 + T_1. \tag{21}$$

The scale height $H = \frac{p_0}{\rho_0 g}$ has been non-dimensionalised in terms of the length $L = c_s\tau$.

In the ideal case, i.e. when no thermal conduction is present, these equations can then be combined to give

$$\frac{\partial^2 v}{\partial t^2} = -g\gamma\frac{\partial v}{\partial z} + c_s^2\frac{\partial^2 v}{\partial z^2}. \tag{22}$$

Assuming that $v(z,t) \sim \sin(\omega t)\exp(ikz)$, we find

$$ik = \frac{1}{2H} \pm \frac{i}{c_s}\sqrt{\omega^2 - \omega_c^2}, \tag{23}$$

where $\omega_c = \frac{g\gamma}{2c_s}$ is the cut-off frequency. This implies that the velocity perturbations in an ideal, stratified plasma are given by

$$v(z,t) \sim \sin(\omega t)e^{z/2H}e^{\frac{i}{c_s}z\sqrt{\omega^2-\omega_c^2}}, \tag{24}$$

which is in agreement with Roberts (1985). From Eq. (24), we expect the amplitudes of the velocity perturbations to increase as $\exp(z/2H)$ when gravitational stratification is included in the model. Note here that the observed periods are of the order of 200−400 s (De Moortel et al. 2002a), and hence, for typical coronal values (see Eq. (7)), the observed frequencies are larger than the cut-off frequency ω_c, which implies that the observed disturbances would indeed be propagating in a stratified, coronal atmosphere.

Figure 2a shows a cross-section of the perturbed velocity as a function of z at a constant time. No thermal conduction was included, i.e. $d = 0$. A coronal scale height of 50 Mm, which corresponds to a dimensionless scale height of $H = 1.1$ was used. The dashed line corresponds to a similar result in an unstratified medium. It is clear that including gravitational stratification causes the amplitude of the velocity perturbations (solid line) to increase rapidly, whereas the amplitude of the perturbations in non-stratified atmosphere (dashed line) remain constant. The dot-dashed line confirms the $\exp(z/2H)$ growth rate of the amplitudes that we obtained in Eq. (24). In Fig. 2b, we look at the combination of stratification and thermal conduction, with the thermal ratio $d = 0.025$. Although the growth rate

of the pertubations is somewhat slower than $\exp(z/2H)$ (from more than 250% of the initial value at 100 Mm, to about 130%, Table 1), the amplitudes are still increasing for the standard value of the thermal ratio d.

4. Diverging magnetic field geometry

In order to investigate the effects of a diverging magnetic field geometry, we introduce a field-aligned coordinate s. We also remind the reader that, in this paper, z always denotes the vertical (Cartesian) coordinate and r the (spherical) radial coordinate. We will consider the gravitational acceleration used by Tsiklauri & Nakariakov (2001). These authors study a semi-circular loop of curvature radius R_L and take into account the effects of a non-zero inclination angle α and a non-zero offset Z_0 of the loop centre from the base of the corona (i.e. the loop does not necessarily have to be a half circle, but can be any segment of a circle). We will extend the model investigated by Tsiklauri & Nakariakov (2001) by including the effect of area divergence. So far, propagating intensity disturbances have mainly been observed in the lower parts of large coronal loops, i.e. in the first about 50 Mm (De Moortel et al. 2002a). Therefore, we will assume that the field-aligned length scales we are interested in, are considerably smaller than the radius of the Sun and hence, that we can neglect the denominator in Eq. (1) of Tsiklauri & Nakariakov (2001). The gravitational acceleration along the loop is then given by $g(s) = g\cos\alpha G(s)$, where

$$G(s) = \sqrt{1-\frac{Z_0^2}{R_\mathrm{L}^2}}\cos\left(\frac{s}{R_\mathrm{L}}\right) - \frac{Z_0}{R_\mathrm{L}}\sin\left(\frac{s}{R_\mathrm{L}}\right). \tag{25}$$

Accordingly, the equilibrium density profile along the loop is given by

$$\rho_0(s) = \exp\left\{-\frac{1}{H}\cos\alpha\left[\sqrt{R_\mathrm{L}^2-Z_0^2}\sin\left(\frac{s}{R_\mathrm{L}}\right) + Z_0\left(\cos\left(\frac{s}{R_\mathrm{L}}\right)-1\right)\right]\right\}. \tag{26}$$

Note that we can recover the standard, "vertically" stratified model by letting $\alpha \to 0$, $Z_0 \to 0$, and $R_\mathrm{L} \to \infty$, in which case $s \to z$, $g(s) \to g$ and $\rho_0(s) \to \rho_0(z) \sim \exp(-z/H)$.

Using Eqs. (25) and (26), the linearised, dimensionless MHD equations, including gravitational stratification, thermal conduction and a diverging field, can be written as

$$\frac{\partial v_1}{\partial t} = -\rho_0^{-1}\frac{1}{\gamma}\frac{\partial p_1}{\partial s} - \rho_0^{-1}\frac{1}{\gamma H}\rho_1\cos\alpha G(s), \tag{27}$$

$$\frac{\partial \rho_1}{\partial t} = -v_1\frac{\partial \rho_0}{\partial s} - \rho_0\frac{1}{A(s)}\frac{\partial}{\partial s}(A(s)v_1), \tag{28}$$

$$\frac{\partial T_1}{\partial t} = -(\gamma-1)\rho_0\frac{1}{A(s)}\frac{\partial}{\partial s}(A(s)v_1) + \frac{\gamma d}{A(s)}\frac{\partial}{\partial s}\left(A(s)\frac{\partial T_1}{\partial s}\right), \tag{29}$$

$$p_1 = \rho_1 + T_1, \tag{30}$$

where s has been non-dimensionalised in terms of a field-aligned length, $S = c_\mathrm{s}\tau$, and where $A(s)$ is a general cross-sectional area of the loop. We will now look at several different cases: firstly, we will set $H = \infty$, $\alpha = 0$, $Z_0 = 0$, and $R_\mathrm{L} = \infty$ and consider purely radial divergence, i.e. $A(s) \sim s^2$ (Sect. 4.1), and a more general area divergence (Sect. 4.2), where $A(s)$ is determined from observed coronal loops. Afterwards, we will consider the case $H \neq \infty$ and investigate the combination of (general) area divergence and (vertical) gravitational stratification (Sect. 4.3). Finally, we will include loop curvature and non-zero loop offset and inclination (Sect. 4.4).

4.1. Radial divergence

In a first instance, we look at radial divergence, i.e. we consider a background magnetic field of the form $\boldsymbol{B_0} = \left(B_0\frac{R_\mathrm{o}^2}{r^2}, 0, 0\right)$, where r is the radial coordinate of a standard spherical coordinate system, and R_o is the solar radius. The governing equations for this system can be obtained by replacing the field-aligned coordinate s by the radial coordinate r and the general area divergence $A(s)$ by r^2 in Eqs. (27) to (30), with $H = \infty$, $\alpha = 0$, $Z_0 = 0$, and $R_\mathrm{L} = \infty$. In the ideal case, i.e. when no thermal conduction is present, these equations can then be combined to give

$$\frac{\partial^2 v}{\partial t^2} - \frac{\partial^2 v}{\partial r^2} - \frac{2}{r}\frac{\partial v}{\partial r} + \frac{2}{r^2}v = 0. \tag{31}$$

Assuming that $v(r,t) \sim \sin(\omega t)V(r)$, this equation can be re-written as

$$r^2\frac{\mathrm{d}^2V}{\mathrm{d}r^2} + 2r\frac{\mathrm{d}V}{\mathrm{d}r} + \left(\omega^2r^2 - 2\right)V = 0, \tag{32}$$

which is the equation for the spherical Bessel functions. Hence, the perturbed velocity will be of the form

$$v(r,t) = \sin(\omega t)\left[C_1 j_1(\omega r) + C_2 y_1(\omega r)\right], \tag{33}$$

where the constants C_1 and C_2 can be determined from the boundary conditions. For large arguments, the first order spherical Bessel functions $j_1(\omega r)$ and $y_1(\omega r)$ will behave as $(\omega r)^{-1}$.

Figure 3a shows a cross-section of the perturbed velocity as a function of r at a specific time, in an ideal (no thermal conduction), radially diverging plasma. The dashed line shows the result in a non-diverging plasma. Using the normalisation $R = c_\mathrm{s}\tau$ and the values given by Eq. (7), we find $R_\mathrm{o} \approx 14$. Comparing the solid (diverging) and dashed (non-diverging) lines, it is clear that the amplitudes of the perturbed velocity decrease with height in the diverging medium. From Table 1, we see that, at 100 Mm, the amplitudes have been reduced by less than 15% due to the (radial) area divergence. Note however, that this is not true dissipation, as there is no dissipation mechanism present. The divergence of the magnetic field lines merely causes the amplitude of the perturbations along a given field line to decrease. Finally, the dot-dashed line in Fig. 3a confirms the r^{-1} amplitude decrease, as was predicted above from the behaviour of the first order Bessel functions.

In Fig. 3b, we have combined the effects of radial divergence and thermal conduction, using the thermal ratio $d = 0.025$. The dashed line shows the perturbed velocity in the non-diverging case, with the same amount of thermal conduction present. The figure shows that the amplitude decrease due to the divergence of the field lines is small compared to the amplitude decay due to thermal conduction. The radial divergence

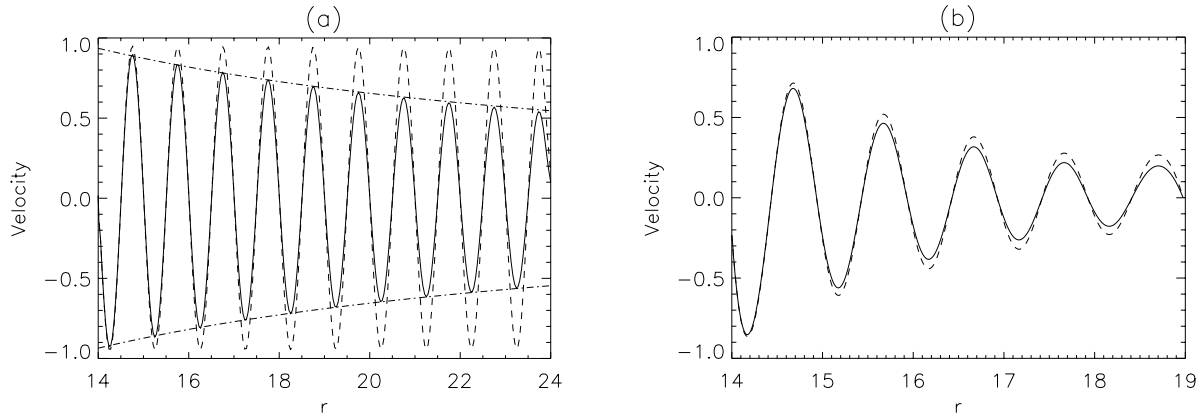

Fig. 3. a) A cross-section of the perturbed velocity as a function of r at $t = 10$, for which $r_{\max} = R_o + 15$ and $d = 0$ and for which the boundary was driven continuously. The dashed line shows the result for a non-diverging field. The dot-dashed line shows the $1/r$ decay rate. **b)** Similar to **a)** but at $t = 5$ and with $r_{\max} = R_o + 5$ and $d = 0.025$.

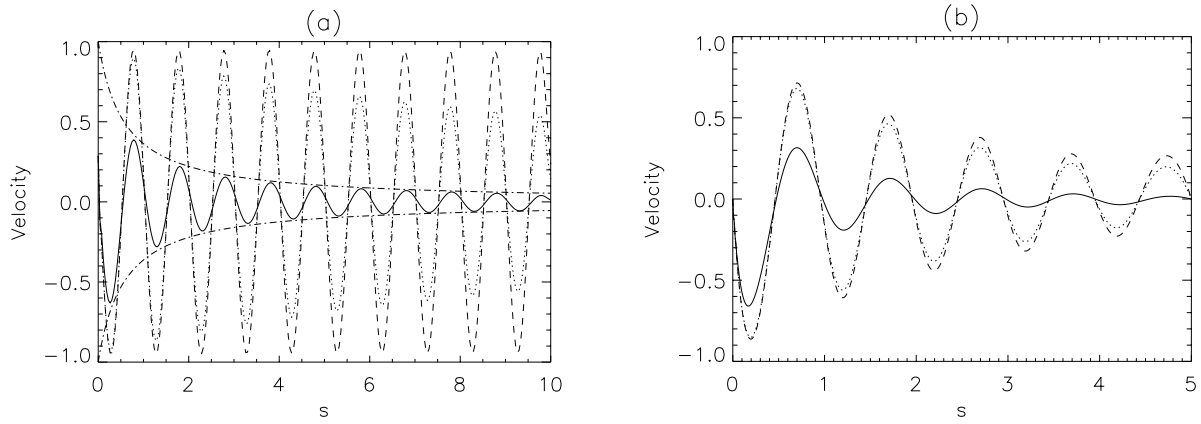

Fig. 4. a) A cross-section of the perturbed velocity as a function of s at $t = 10$, for which $s_{\max} = 15$ and $d = 0$ and for which the boundary was driven continuously. The dashed line shows the result for a non-diverging field and the dotted line corresponds to a radially diverging field. The dot-dashed line shows the $A(s)^{-1/2}$ decay rate. **b)** Similar to **a)** but at $t = 5$ and with $s_{\max} = 5$ and $d = 0.025$. In both cases, we took $r_0 = 5$ Mm and $\theta = 10$ deg.

causes some additional reduction (about 6% at 100 Mm) of the amplitude but the effect is small. Given our previous results (Paper I), it is unlikely that a combination of radial divergence and "standard" thermal conduction can explain the rapid decay of the slow MHD waves observed in coronal loops.

4.2. General area divergence

In this section, we use Eqs. (27) to (30) (again with $H = \infty$, $\alpha = 0, Z_0 = 0$, and $R_L = \infty$), to look at the effect of a more general area divergence on the propagation of slow MHD waves in coronal loops. As in De Moortel et al. (2003), we define the cross-sectional area of a coronal loop as

$$A(s) = \pi(r_0 + s\tan(\theta))^2, \tag{34}$$

where r_0 is the radius at the base of the loop and θ is the expansion angle.

Figure 4a shows a cross-section of the perturbed velocity as a function of the distance along the loop s, at $t = 10$. The dotted line shows a similar result in a radially diverging field, whereas the dashed line corresponds to a non-diverging field. For the chosen parameters, $r_0 = 5$ Mm and $\theta = 10$ degrees, the amplitudes of the velocity perturbations decrease considerably quicker, compared to the radially diverging case. Indeed, at 100 Mm, the amplitudes have decreased to 19.6% of their initial value, as opposed to 86.3% in the radial case (see Table 1). Guided by the decay rate obtained in Sect. 4.1, for a radially diverging field, we expect the general decay rate to behave as $1/\sqrt{A(s)}$. Indeed, the dot-dashed line in Fig. 4a confirms that a decay $\sim A(s)^{-1/2}$ is a very good fit for the amplitude decrease of the velocity perturbations. However, in Sect. 4.1 we found that the amplitude decrease due to the *radial* divergence of the field was very small compared to the damping due to thermal conduction. In contrast, Fig. 4b shows that the general area divergence (with the chosen parameters) does contribute significantly to the amplitude decrease of the perturbations, even if thermal conduction is included. Indeed, if we compare the solid (diverging) and dashed (non-diverging) lines, we see that there is a considerable additional decay (of the order of 35%) due to the field line divergence. Comparing the dotted (radially diverging) and dashed (non-diverging) lines, it is clear that this is not the case for a radially diverging field. So far, the effects of (normal) compressive viscosity (see Paper I), optically thin radiation, gravitational stratification and radial divergence

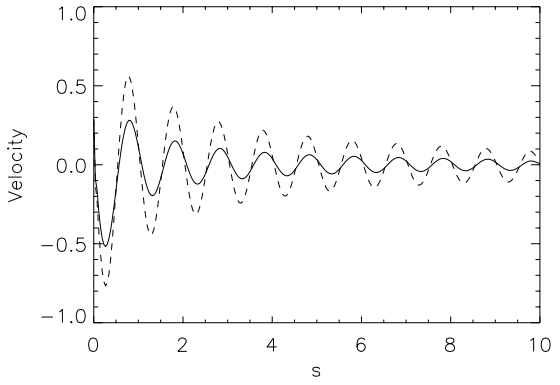

Fig. 5. A cross-section of the perturbed velocity as a function of s at $t = 10$, for which $s_{\max} = 15$, $d = 0$, $r_0 = 5$ Mm and the expansion angle $\theta = 15$ degrees. The dashed line shows the result for an expansion angle $\theta = 5$ degrees.

have not been very encouraging, given that the observed perturbations damp more rapidly than can be explained by thermal conduction alone. However, it seems that a more general area divergence can cause a significant, additional, decrease of the amplitudes of the perturbations.

Given the good fit of the estimated $A(s)^{-1/2}$ decay rate, where $A(s)$ is the cross-sectional area of the loop, we expect the amplitudes of the perturbations to decrease quicker for larger $A(s)$. Therefore, increasing the expansion angle θ should result in a more rapid decline of the perturbation amplitudes. In Fig. 5 we compare the perturbed velocity at a given time ($t = 10$) for an expansion angle $\theta = 15$ degrees (solid line) and $\theta = 5$ degrees (dashed line), respectively. It is obvious that the larger expansion angle results in a much more rapid amplitude decrease. As the cross-sectional area (Eq. (34)) can be re-written as

$$A(s) = \pi r_0 \left(1 + s\frac{\tan(\theta)}{r_0}\right)^2, \tag{35}$$

varying the width r_0 at the base of the loop will basically have the same effect as varying the divergence angle θ.

4.3. Divergence and stratification

We now look at the combination of a general area divergence and (vertical) gravitational stratification, by setting $H \neq \infty$ in Eqs. (27) to (30) (but still keeping $\alpha = 0$, $Z_0 = 0$, and $R_{\rm L} = \infty$). So far, we have shown that stratification results in an increase of the perturbations amplitudes, with an $\exp(z/2H)$ growth rate, where H is the gravitational scale height. On the other hand, the divergence of the background magnetic field causes the amplitudes to decrease as $A(s)^{-1/2}$, where $A(s)$ is the cross-sectional area of the loop. Therefore, we expect that the combined effect of stratification and divergence on the damping of the slow waves will depend strongly on the choice of the actual divergence parameters (r_0 and θ). Note here that, as we are not considering loop curvature, offset or inclination, that the field-aligned coordinate s is essentially vertical, and therefore the same as the Cartesian coordinate z.

Figure 6a shows a cross-section of the perturbed velocity as a function of the distance along the loop s, at $t = 10$. The dashed line shows the corresponding velocity in a non-stratified, diverging field. Although there is an initial decrease, the amplitudes rapidly increase due to the decreasing background density. However, comparing this result with Fig. 2a, it is clear that the amplitude increase is slowed down considerably by the area divergence. The dot-dashed line shows that $\exp(s/2H) \times A(s)^{-1/2}$, i.e. a combination of the stratification growth rate and the divergence decay rate, provides a good estimate of the amplitude variation along the loop. The estimate of the variation of the amplitude also shows that no matter how large we make the divergence angle θ (which would increase the amplitude decay due to the divergence), the effect of stratification will eventually become more important and cause the amplitudes to increase again.

Figure 6b shows the combined effect of gravitational stratification, area divergence and thermal conduction. As expected from the ideal result, including stratification (solid line) results in a slower decay of the perturbations, compared to a combination of thermal conduction and area variation (dashed line). However, it is encouraging to see that the amplitude decrease is still faster (26.1% at 100 Mm) than would be the case for thermal conduction alone (46.8% at 100 Mm), i.e. no stratification or area divergence (dotted line). If we increase the rate of divergence, by increasing the expansion angle θ, the basic result does not change, i.e. the amplitudes decrease is quickest when area divergence is combined with thermal conduction, without gravitational stratification.

4.4. Loop curvature and inclination

Finally, we add the effects of loop curvature ($R_{\rm L} \neq \infty$), non-zero offset ($Z_0 \neq 0$) and non-zero inclination ($\alpha \neq 0$) to the model. Note that the field-aligned coordinate s is now fundamentally different from the "vertical" coordinate z. However, as already pointed out above, most of the propagating intensity disturbances have been observed in the lower parts of large coronal loops. Therefore, for this specific class of coronal loops, actual values of α, Z_0 and $R_{\rm L}$ are largely unknown. For our simulations, we chose $R_{\rm L} = 600$ Mm, based on the average of the values quoted by Reale et al. (2000) and Robbrecht et al. (2001). Similar to Tsiklauri & Nakariakov (2001), we take $Z_0 = 60$ Mm, based on the "average" EUV loop (Aschwanden et al. 1999). The inclination angle α is taken to be 30 degrees, according to the estimates of De Moortel et al. (2003) and Robbrecht et al. (2001). The results of these simulations are shown in Fig. 7.

Figures 7a and 8 show a cross-section of the perturbed velocity as a function of the distance along the loop s, when no thermal conduction is included. A comparison with "vertical" stratification (dashed line) shows clearly that non-zero inclination and the offset reduce the growth of the perturbation amplitudes due to gravitational stratification, which agrees with the result of Tsiklauri & Nakariakov (2001). On the other, comparing with the corresponding perturbed velocity in a non-stratified, diverging field shows that gravity still has a

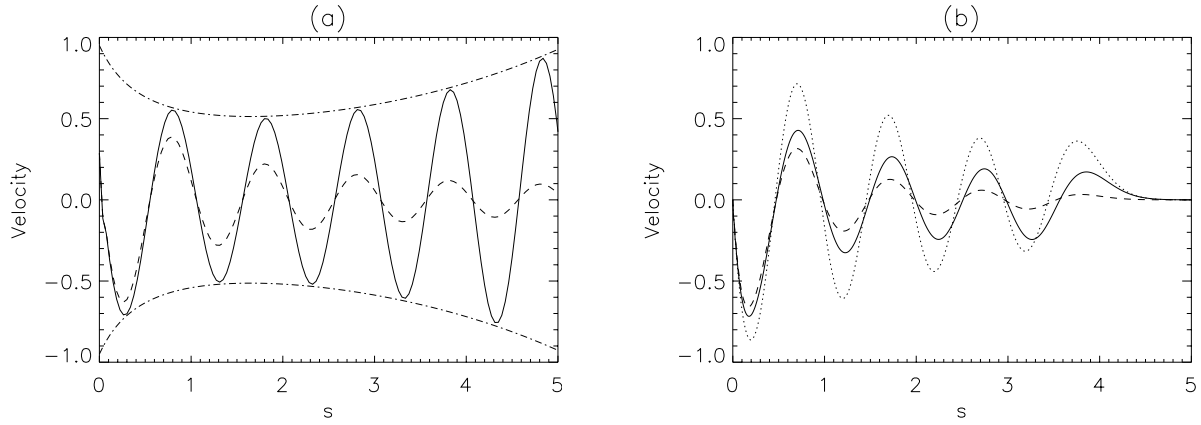

Fig. 6. a) A cross-section of the perturbed velocity as a function of s at $t = 10$, for which $s_{\max} = 15$ and $d = 0$ and for which the boundary was driven continuously. The dashed line shows the result for a non-stratified (diverging) model. The dot-dashed line shows the $\exp(s/2H)\times A(s)^{-1/2}$ amplitude change. **b)** Similar to **a)** but at $t = 4$ and with $s_{\max} = 5$ and $d = 0.025$. The dotted line corresponds to a model which includes only thermal conduction. In both cases, we took $r_0 = 5$ Mm and $\theta = 10$ deg.

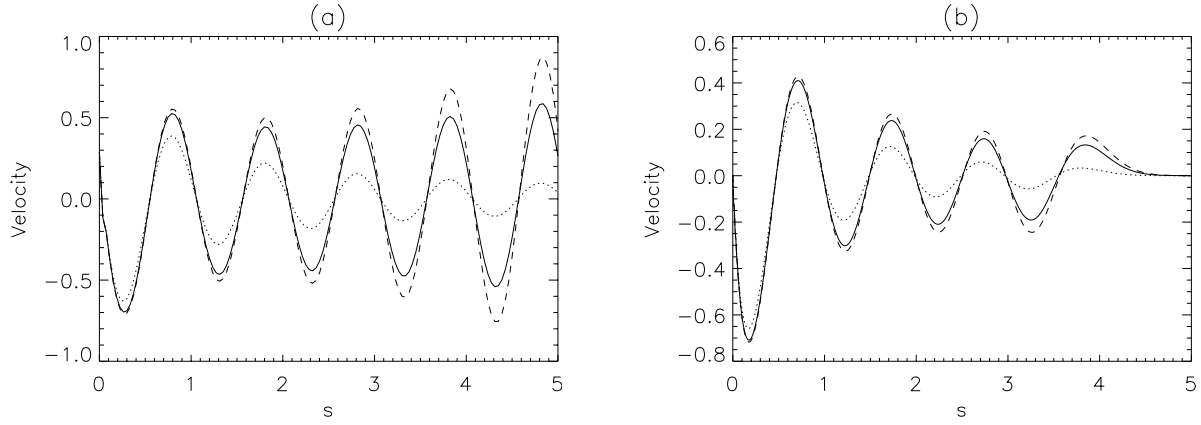

Fig. 7. a) A cross-section of the perturbed velocity as a function of s at $t = 10$, for which $s_{\max} = 15$, $d = 0$, $\alpha = 30$ degrees, $R_{\rm L} = 600$ Mm and $Z_0 = 60$ Mm. The dashed line shows the result for a "vertically" stratified, diverging model, whereas the dotted line corresponds to a non-stratified (diverging) model. **b)** Similar to **a)** but at $t = 4$ and with $s_{\max} = 5$ and $d = 0.025$. In both cases, we took $r_0 = 5$ Mm and $\theta = 10$ deg.

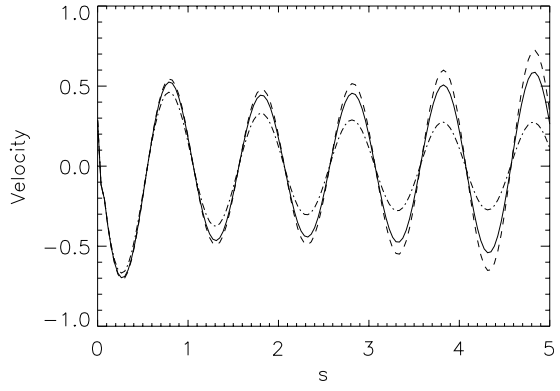

Fig. 8. A cross-section of the perturbed velocity as a function of s at $t = 10$, for which $s_{\max} = 15$, $d = 0$, $r_0 = 5$ Mm, $\theta = 10$ degrees $R_{\rm L} = 600$ Mm and $Z_0 = 60$ Mm. The solid line corresponds to an inclination angle $\alpha = 30$ degrees, whereas the dashed and dot-dashed lines correspond to $\alpha = 15$ degrees and $\alpha = 60$ degrees, respectively.

significant effect on the wave amplitudes. Figure 7b shows the results for which thermal conduction was included in the model, and the basic conclusion is the same as in the ideal case, namely that a non-zero inclination and offset reduce the effect of gravity on the perturbation amplitudes.

5. Comparison with observations

In this section, we compare the results obtained above with observations of oscillations in solar coronal loops, which were interpreted in terms of slow magneto-acoustic waves. The density disturbances were observed by TRACE in the lower part of large, coronal loops, close to active regions (De Moortel et al. 2002a). The amplitudes of the intensity oscillations were roughly 4.1 ± 1.5% of the background loop brightness, with the smallest amplitudes detected above a 99% confidence level of the order of 1%. The amplitudes of the propagating disturbances were found to decrease very quickly and were usually only observed in the first 8.9 ± 4.4 Mm along the loop (ranging from 2.9−23.2 Mm). Typically, the intensity oscillations are no longer detected, above a 99% confidence level, when the amplitudes have decreased by a factor of about four. Therefore, rather than a damping length, we will estimate a "detection" length,

Table 2. Overview of the oscillations found in the JOP 83 & JOP 144 TRACE data in the 171 Å bandpass; t_0 is the date and the start time of the observation sequence, r_0 is the estimate of the radius at the base of the loop and θ is the estimated expansion angle.

Loop	t_0	r_0 (Mm)	θ (degrees)	Loop	t_0	r_0 (Mm)	θ (degrees)
1a	230399 0653	1.5–2.5	10–15	13c	060601 0650	1.4–2.1	11–15
2a	040400 0928	0.6–1.25	0–5	13d	060601 0650	0.7–1.4	3–7
3a	050400 0230	1.25–1.9	5–12	13e	060601 0650	0.7–1.4	10
4a	070400 1328	0.6–1.25	5–7	13f	060601 1006	1.4–2.1	9
4b	070400 1151	1.25–1.9	2	13g	060601 1006	2.1–2.8	11–13
4c	070400 1242	1.25–1.9	7–9	14a	070601 0836	3.2–4.2	12–16
4d	070400 1328	1.4–2.1	5–8	14b	070601 0836	0.9–1.8	6–7
5a	080400 1204	0.7–1.4	3–5	14c	070601 1314	1.1–2.1	4–6
6a	090400 1354	1.4–2.1	3–5	14d	070601 1314	1.1–2.1	3
7a	110400 1514	0.7	3–10	14e	070601 1314	2.1–2.9	7–22
7b	110400 1514	0.7–1.3	6	14f	070601 1314	1.4	2–7
7c	110400 1514	1.3	5–10	15a	090601 0828	1.4	2
8a	130400 1405	1.4	4–5	16a	120601 0725	1.0–1.9	2
9a	170400 1325	1.25–1.9	4–5	16b	120601 0725	1.0-1.9	5–13
10a	180400 2330	1.25–1.9	8–12	17a	130601 0138	1.6	2–3
11a	190400 1535	0.6–1.25	2–3	17b	130601 0646	1.2–2.1	4–5
12a	050601 0637	1.7–2.5	7–11	17c	130601 0646	1.7–2.5	11–12
13a	060601 0650	1.4–2.1	6-13	17d	130601 0646	0.8	4–9
13b	060601 0650	1.4–2.1	11–20	17e	130601 1300	1.7	4–6

where the density perturbations have decreased by a factor of four, as we did in Paper I.

However first of all, we have to obtain an estimate of the actual divergence rate of the coronal loops in which propagating slow waves were observed. To determine the area expansion of the loop, we follow the same procedure as De Moortel et al. (2003), i.e. intensity contours are used to determine the radius of the loops. When possible, a closed contour is used (in case of an isolated loops), otherwise, a dip in the intensity contours is followed (when the loop is not sufficiently isolated). In Table 2, an overview is given of the estimates of the radius at the base of the loops (r_0) and the estimated expansion angles (θ) for all loops analysed in De Moortel et al. (2002a). We find an average width $r_0 = 1.6 \pm 0.37$ Mm (range of 0.7−3.7 Mm) and expansion angle $\theta = 7.1 \pm 3.8$ degrees (range of 2−15.5 degrees).

For these simulations, we used a thermal ratio $d = 0.25$, which corresponds to the standard, coronal thermal conduction coefficient and a dimensionless scale height $H = 1.1$, which corresponds to an actual gravitational scale height of about 50 Mm. We use an initial loop width $r_0 = 1.6$, and divergence angle $\theta = 7.1$ degrees, as determined from the observations. Compressive viscosity and optically thin radiation do not contribute significantly to the dissipation for the chosen conditions and hence, were not included in the model. Furthermore, the effects of loop curvature, offset and inclination were not taken into account (setting $\alpha = 0$, $Z_0 = 0$, and $R_L = \infty$), as actual values for these parameters are at best uncertain (and usually unknown) for the loops in which oscillations were observed.

Figure 9a shows a contour plot of the perturbed density, as a function of length along the loop (in Mm) and time (in minutes). The contour level where the density has decreased to a quarter of its initial value is outlined seperatly. We see that in this case, the perturbations would only have been detected in the first 10−15 Mm along the loop, which is in good agreement with the observed values. We recall here that (standard) thermal conduction alone resulted in a detection length of the order of 130 Mm (see Paper I). Area divergence causes a very significant, additional decrease of the amplitudes, even when gravitational stratification is included, and combined with thermal conduction, could potentially explain the rapid decay of the observed intensity perturbations. At present, we have not considered the effect of loop curvature, offset or inclination. However, in Sect. 4.4 we showed that including these loop properties in the model results in a further reduction of the perturbation amplitudes. Therefore, the simulations that we compared with the observations in this section could be considered as a "worst case" scenario. Another factor that might affect the detection length is the angle between the loop and the line of sight. This viewing angle will be determined by a combination of the loop orientation and inclination, and its location on the solar disc. Depending on the viewing angle, the observed (projected) detection length could be shorter or longer than the actual detection length. Without additional information about the actual geometry of the observed loops, it is almost impossible to make any definite conclusions on the viewing angle. However, we do expect the actual detection lengths to be of the same order of magnitude as the observed, projected detection lengths.

In Fig. 9b, we show a cross-section of the perturbed density along the loop, at $t = 14$ min, which corresponds roughly to the middle of a typical observational sequence. At this given time,

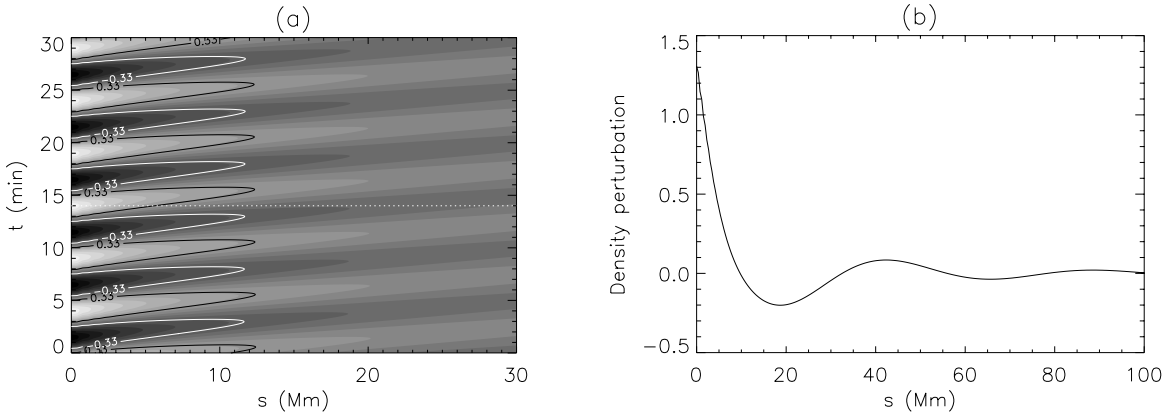

Fig. 9. a) Contour plot of the perturbed density as a function of s and t, for which $d = 0.1$, $r_0 = 1.6$ Mm and $\theta = 7.1$ degrees and for which the boundary was driven continuously. **b)** A cross-section of the perturbed density as a function of s at $t \approx 14$ min (dotted line).

there would be a strong density perturbation near the (coronal) footpoint of the loop, and a few, progressively weaker, disturbances further along the loop, which corresponds well with the observed pattern of intensity perturbations.

6. Discussion and conclusions

In this paper, we have investigated the behaviour of slow MHD waves in a stratified and diverging atmosphere, to complete our study of the decay of slow MHD waves in a 1D model. From Paper I and Sect. 2, it became apparent that neither compressive viscosity nor optically thin radiation are an effective dissipation mechanism under the observed coronal conditions, i.e. at 1 MK. Although the reference height of 100 Mm was chosen arbitrarily, a relative comparison of all the different effects can be found in Table 1. Thermal conduction is the most efficient dissipative mechanism, but as we pointed out in Paper I, there is a minimum damping length that can be obtained with thermal conduction alone. Furthermore, to obtain this minimum damping length, we had to enhance the "standard" coronal thermal conduction coefficient by a factor of about 4. Using this enhanced thermal conduction, we obtained detection lengths that are comparable in order of magnitude to the observed detection lengths. However, if we want to use the standard thermal conduction coefficient, a further decrease of the perturbation amplitudes was needed to explain the observed detection lengths. We also point out that at higher temperatures, damping due to thermal conduction will reduce with increasing temperature, until eventually the waves propagate largely undamped, at the (slower) isothermal sound speed. On the other hand, compressive viscosity could become a more effective and significant dissipation mechanism at higher temperatures (Ofman et al. 2000b).

Including gravitational stratification causes a considerable increase of the wave amplitudes as they propagate along the loop, due to the decreasing background density. Although the reduction of the amplitudes due to radial area divergence was not sufficient to counter balance the effect of gravity, we found that a more general field divergence not only balances the effect of gravity, but causes a significant additional decrease of the amplitudes. We remind the reader again that the decrease of the perturbations due to area divergence is not true dissipation, as there is no dissipative mechanism present. A comparison with observations showed that a combination of (vertical) stratification, area divergence and (standard) thermal conduction yielded detection lengths that are comparable with observed values. Including loop curvature, an offset of the loop centre from the base of the corona and inclination with respect to the vertical resulted in a further decrease of the perturbations amplitudes, as these factors reduce the effect of gravity along the loop.

So far, we have only considered a one dimensional loop model, in order to study the effect of each of the dissipation mechanisms, gravity and loop geometry separately. Together with the results from Paper I, we have now more or less exhausted the possibilities of a 1D, isothermal, loop model. Extending the model to two dimensions would allow us to include several other loop properties that might influence the wave damping. For example, including a density profile that varies across the loop could result in the excitation of different MHD modes and hence energy could leave the system as it is transferred to a different wave mode. This mode coupling due to an inhomogeneous density profile will be investigated in a third paper in this series on the damping of slow waves in coronal loops. Additional effects such as phase mixing or resonant absorption could also occur, causing additional dissipation and hence, shorter damping lengths.

References

Aschwanden, M. J., Newmark, J. S., Delaboudiniere, J.-P., et al. 1999, ApJ, 525, 842
Berghmans, D., & Clette, F. 1999, Sol. Phys., 186, 207
Brynildsen, N., Maltby, P., Fredvik, T., & Kjeldseth-Moe, O. 2002, Sol. Phys., 207, 259
DeForest, C. E., & Gurman, J. B. 1998, ApJ, 501, L217
Del Zanna, L., Hood, A. W., & Longbottom, A. W. 1997, A&A, 318, 963
De Moortel, I., Ireland, J., & Walsh, R. W. 2000, A&A, 355, L23
De Moortel, I., Ireland, J., Hood, A. W., & Walsh, R. W. 2002a, Sol. Phys., 209, 61
De Moortel, I., Hood, A. W., Ireland, J., & Walsh, R. W. 2002b, Sol. Phys., 209, 89

De Moortel, I., Ireland, J., Hood, A. W., & Walsh, R. W. 2002c, A&A, 387, L13
De Moortel, I., & Hood, A. W. 2003, A&A, 408, 755
De Moortel, I., Parnell, C. E., & Hood, A. W. 2003, Sol. Phys., 215, 69
Erdélyi, R. 1996, Ph.D. Thesis, K. U. Leuven
Field, G. B. 1965, ApJ, 142, 531
Hood, A. W., & Priest, E. R. 1980, A&A, 87, 126
King, D. B., Nakariakov, V. M., Deluca, E. E., Golub, L., & McClements, K. G. 2003, A&A, 404, L1
Marsh, M. S., Walsh, R. W., De Moortel, I., & Ireland, J. 2003, A&A, 404, L37
Nakariakov, V. M., Verwichte, E., Berghmans, D., & Robbrecht, E. 2000, A&A, 362, 1151
Ofman, L., Romoli, M., Poletto, G., Noci, C., & Kohl, J. L. 1997, ApJ, 491, L111
Ofman, L., Nakariakov, V. M., & DeForest, C. E. 1999, ApJ, 514, 441
Ofman, L., Romoli, M., Poletto, G., Noci, C., & Kohl, J. L. 2000a, ApJ, 529, 592
Ofman, L., Nakariakov, V. M., & Sehgal, N. 2000b, ApJ, 533, 1071
O'Shea, E., Muglach, K., & Fleck, B. 2002, A&A, 387, 642
Porter, L. J., Klimchuk, J. A., & Sturrock, P. A. 1994, ApJ, 435, 482
Porter, L. J., Klimchuk, J. A., & Sturrock, P. A. 1994, ApJ, 435, 502
Reale, F., Peres, G., Serio, S., DeLuca, E. E., & Golub, L. 2000, ApJ, 535, 412
Robbrecht, E., Verwichte, E., Berghmans, D., et al. 2001, A&A, 370, 591
Roberts, B. 1985, in Solar System Magnetic Fields, ed. E. R. Priest (Dordrecht: Reidel), 3
Roberts, B. 2000, Sol. Phys., 193, 139
Roberts, B. 2003, in Turbulence, Waves and Instabilities in the Solar Plasma, ed. R. Erdélyi et al. (Kluwer), Nato Sci. Ser., 124
Roberts, B., Edwin, P. M., & Benz, A. O. 1984, ApJ, 279, 857
Tsiklauri, D., & Nakariakov, V. M. 2001, A&A, 379, 1106